First-principles study of $In_2X_2O_7$ (X=C, Si, Ge, and Sn) compounds

S.Zh.Karazhanov[1,2*], P.Ravindran[2], and U. Grossner[3]

[1]*Centre for Material Science and Nanotechnology, Department of Chemistry, University of Oslo, PO Box 1033 Blindern, N-0315 Oslo, Norway*

[2]*Physical-Technical Institute, 2B Mavlyanov St., 700084 Tashkent, Uzbekistan*

[3]*Department of Physics, University of Oslo, P.O. Box 1048 Blindern, N-0316 Oslo, Norway*

Abstract

This work presents a study of structural properties, electronic structure, chemical bonding, and optical spectra of polymorphs of $In_2X_2O_7$ (X=C, Si, Ge, and Sn) by first-principles calculations. Only monoclinic phase of $In_2Ge_2O_7$ is known in scientific literature. Cubic and monoclinic phases of $In_2Si_2O_7$ are well known. Using positional and lattice parameters for cubic $In_2Si_2O_7$ we studied ground state properties of $In_2Ge_2O_7$. From the study of ground state properties we found that upon compressing monoclinic phase of both of the compounds can be transformed into cubic phase. Cubic phase of $In_2Si_2O_7$ is found to be more stable than the monoclinic phase. However, monoclinic phase of $In_2Si_2O_7$ is more stable than the cubic phase. So far, both $In_2Ge_2O_7$ and $In_2Si_2O_7$ have commonly been used as scintillation materials. From the study of electronic structure and optical spectra we found that these materials posses the features of transparent conducting oxides.

Keywords: $In_2C_2O_7$, $In_2Si_2O_7$, $In_2Ge_2O_7$, $In_2Sn_2O_7$, optical properties, scintillators.

PACS: 71.15.-m; 71.22.+i

[2]Present address: *Institute for Energy Technology, NO-2027 Kjeller, Norway*

1. Introduction

Studies of the indium-rich compounds became attractive because of the possibility of many technologically useful applications such as, e.g., high density, high light output scintillators,[1] and photovoltaics (PV).[2-5] Here we study the indium-related compounds of type $In_2X_2O_7$ (X=C, Si, Ge, and Sn) by the first-principles calculations. Among them $In_2Si_2O_7$ and $In_2Ge_2O_7$ present interest as fast, high output of light, and low afterglow scintillators for computer tomography imaging and similar applications.[6] The compounds are reported[7] as important catalyst materials, scintillators for detection of low-energy solar neutrinos in agreement with Raghavan's nuclear reaction, and porous ceramic materials for humidity sensors. Recently, $In_2Si_2O_7$ and $In_2Ge_2O_7$ have raised interest in photovoltaics (PV) as well[2-5] in connection with one of the concepts of the 3rd-generation PV related to usage of quantum dots. The dots are suggested to be important for efficiency improvements of solar cells by tuning the band gap, optical properties of the matrix compound, cooling of hot charge carrier, etc.[5] The compounds $In_2X_2O_7$ can be formed at the interface in between two matrixes as intermediate layer. For example, in studies of the role of the Ge based quantum dots embedded into indium-tin-oxide (ITO) In_2O_3:Sn, an intermediate layer has been detected by XRD in between Ge dots and ITO, which is suggested to be $In_2Ge_2O_7$.[3-4] There are many reports about $In_2Sn_2O_7$ formed in between ITO and glass,[8] in the In_2O_3-SnO_2,[9] and CdTe/CdS/ITO/glass[10] systems, etc. Formation of such an intermediate layers is the issue of materials interaction. When two materials are brought together, solid state reaction and mixing processes can take place might take place, which lead to formation of an alloy at the interface. From this point of view one can suggest that $In_2Si_2O_7$ and $In_2Sn_2O_7$ can be formed in between Si and

In_2O_3:Sn. Although the knowledge of structural, electrical and optical properties of such intermediate layers is important there is no systematic study of this point.

Some of the $In_2X_2O_7$ compounds have been synthesized and studied. For example, tubes of $In_2Ge_2O_7$ have been synthesized with sub-micrometer diameters, which is of the same order of magnitude as the wavelength and mean free path of photons.[11] $In_2Ge_2O_7$ is suggested to find interesting applications as waveguides or micro lasers. Large-scale $In_2Ge_2O_7$ nanobelts have been successfully synthesized by a simple thermal evaporation method without the presence of catalyst and a strong and broad violet emission peak at about 410 nm was observed.[12] $In_2Si_2O_7$ and $In_2Ge_2O_7$ are suggested[1, 13]to be used as radiation detectors with high light output, good attenuation power, low level of afterglow, and fast scintillation decay time.

Another point to be mentioned is that three different structural modifications of $In_2Si_2O_7$ and $In_2Ge_2O_7$ have been observed experimentally. $In_2Si_2O_7$ can be in monoclinic phase[13] and cubic phases whereas $In_2Ge_2O_7$ can be in two different varieties of monoclinic phase.[14-15] There is no structural information regarding the other $In_2X_2O_7$ and possibility of phase transitions between different polymorphs of $In_2X_2O_7$.

The aim of this work is to study ground state properties, electronic structure and optical properties of $In_2Ge_2O_7$ and $In_2Si_2O_7$ in cubic and monoclinic modifications.

2. Computational details

Structural properties, the electronic band structure and optical properties of $In_2X_2O_7$ are studied using the Vienna *ab initio* simulation package (VASP)[16], which calculate the Kohn-Sham eigenvalues within the framework of density functional theory (DFT). The calculations have been performed with the use of the local density

approximation (LDA). The exchange and correlation energy per electron have been described by the Perdew-Zunger parametrization[17] with the quantum Monte Carlo procedure of Ceperley-Alder[18]. The interaction between electrons and atomic cores is described by means of non-norm-conserving pseudopotentials implemented in the VASP package[16]. The pseudopotentials are generated in accordance to the projector-augmented-wave (PAW) method[19-21]. The use of the PAW pseudopotentials addresses the problem of the inadequate description of the wave functions in the core region common to other pseudopotential approaches. The In-4*d*, -5*s*, and -5*p*, O -2*s* and -2*p*, C-2*s* and -2*p*, Si-3*s* and -3*p*, Ge-4*s*, -3*d*, and -4*p*, as well as Sn-5*s*, -4*d*, and -5*p* electrons have been considered as the valence electrons.

$In_2X_2O_7$ studied in this paper are ternary compounds with stoichiometry $In_2B_2O_7$. Four different structural modifications are considered for the compounds with space group (SG) $C1_2/m_1$ (SG number 12) to be denoted hereafter as phase (-*I*), $B112/m$ (SG number 1204), $P12_1/c1$ (SG number 14), and $Fd\bar{3}m$ (SG number 227) denoted as phase (-*II*). Crystal structure and lattice parameters for the first three polymorphs of $In_2X_2O_7$ are almost the same. So, in Fig. 1 we present schematically $In_2X_2O_7$-*I* and -*II*.

In the structural modifications the In and *B* cations are in InO_6 and BO_6 octahedra. Wyckoff positions, lattice parameters, have been provided in Table I. Using the experimentally determined crystal information as input lattice optimization has been performed by the following procedure: Atomic positions, cell volume and shape have been relaxed by force and stress minimization. Crystal structure information obtained from this study was used as input for calculation of the total energy (E_{tot}) as a function of the cell volume (V). The minima (E_{tot}^{min}) of the dependence $E_{tot}(V)$ are taken as the

equilibrium volume. Structural optimization has been performed using a 2×2×2 mesh of the **k**-points and plane-wave cutoff energy 500 eV. The convergence was achieved when the forces acting on the atoms were <20 meV $Å^{-1}$ and the total energy difference between two consecutive iterations were < 10^{-6} eV. The self-consistent calculations have performed for the optimized lattices using a 4×4×4 mesh of special **k**-points and 500 eV plane-wave cutoff energy.

The effective masses for the conduction band (CB) electrons are calculated by:

$$\frac{1}{m_c(\mathrm{k})} = \frac{1}{h^2}\frac{\partial^2 E(\mathrm{k})}{\partial \mathrm{k}^2}\bigg|_{\mathrm{k}=\mathrm{k}_0}, \qquad (1)$$

for a direction k about an extremum point k_0 in the Brillouin zone. As demonstrated later, CB is well dispersive whereas the topmost VB is almost flat. Furthermore, the CB minimum is located at the Γ point. For this reason only CB effective masses have been studied in the close vicinity of the Γ point. For the monoclinic structures the masses have been calculated along the directions Γ→Z and Γ→A. For cubic structures the masses have been studied along Γ→X and Γ→L directions. The band edge energies E(k) have been extracted from DFT calculations and polynomial order higher than 2 was used to achieve best fitting. From the polynomial second order derivative was calculated for the Γ point, which was then used in the effective mass calculations by Eq. (1). Throughout the paper the masses are presented in the unit of the free-electron rest mass m_0.

Imaginary part of the dielectric function $\varepsilon_2(\omega)$ was calculated by the DFT within LDA.

$$\varepsilon_2^{ij}(\omega) = \frac{Ve^2\mathrm{k}}{2\pi\hbar m^2\omega^2}\int d^3\mathrm{k}\sum_{nn'}\langle \mathrm{k}n|p_i|\mathrm{k}n'\rangle\langle \mathrm{k}n'|p_j|\mathrm{k}n\rangle \times f_{\mathrm{k}n}(1-f_{\mathrm{k}n'})\delta(f_{\mathrm{k}n'}-f_{\mathrm{k}n}-\hbar\omega). \qquad (2)$$

Here $(p_x, p_y, p_z) = p$ is the momentum operator, f_{kn} is the Fermi distribution, and $|kn\rangle$ is the crystal wave function, corresponding to energy ε_{kn} with momentum k. For cubic $In_2X_2O_7$ the optical spectra are isotropic; consequently, only one component of the dielectric function is analyzed. However, for monoclinic $In_2X_2O_7$ six components of the optical spectra have been calculated. We concentrate attention only on the three directions **E**||**a**,**b**, and **c**. The real part of the dielectric function $\varepsilon_1(\omega)$ is then calculated using the Kramers-Kronig transformation. These two spectra were then used to calculate all the other optical spectra for the energy range 0-20 eV. In this paper, we presented the reflectivity $R(\omega)$, the absorption coefficient $\alpha(\omega)$, the refractive index $n(\omega)$, and the extinction coefficient $k(\omega)$. More details about the optical calculations are discussed in Ref.[22-23].

3. Results.

3.1. Ground-state properties

Ground state properties of $In_2X_2O_7$ have been studied by DFT. Positional and lattice parameters derived from the calculations for the equilibrium lattices are shown in Table I together with experimentally determined values. After optimization of the lattice structural properties of $In_2X_2O_7$ with space group symmetry $B112/m$ and $P12_1/c1$ are found to be the same as that of $In_2X_2O_7$-I. So, further attention will be focused on $In_2X_2O_7$-I and -II. For the computations the experimentally determined lattice parameters are used as input, which are available only for $In_2Si_2O_7$-I and -II as well as for $In_2Ge_2O_7$-I. However, there are no experimental data for $In_2C_2O_7$-I, -II and $In_2Sn_2O_7$-I, -II. For the latter two compounds respective structural information of the diinidum disilicates have

been used as the input. Analysis of the Table I show that deviation of the calculated equilibrium volumes from the corresponding experimentally determined values are by <1.2% for $In_2Si_2O_7$-I, ~1.0% for $In_2Si_2O_7$-II, and <0.4 % for $In_2Ge_2O_7$-I. The calculated positional parameters from the structural optimization are found to be overall in good agreement with experimental data. Symmetry of the optimized lattice has been compared to that determined experimentally and is found to be the same.

The calculated dependence of the total energy (E_{tot}) as a function of the cell volume (V) for $In_2X_2O_7$-I and -II is presented in Fig. 2. Difference between the equilibrium volumes of $In_2X_2O_7$-I and -II is 26.42 $Å^3$ for $In_2C_2O_7$, 51.61 $Å^3$ for $In_2Si_2O_7$, 51.47 $Å^3$ for $In_2Ge_2O_7$, and 57.47 $Å^3$ for $In_2Sn_2O_7$. Stability of these compounds has been analyzed by comparing total energies between $In_2X_2O_7$-I and -II. $In_2C_2O_7$-II is more stable than $In_2C_2O_7$-I, because total energy of the former is smaller than the latter to ~-10.8 eV. Similarly, E_{tot}^{min} [$In_2Si_2O_7$-I]- E_{tot}^{min} [$In_2Si_2O_7$-II]=0.28 eV. Hence, $In_2Si_2O_7$-II can be said to be more stable than $In_2Si_2O_7$-I. However, E_{tot}^{min} [$In_2Ge_2O_7$-I]- E_{tot}^{min} [$In_2Ge_2O_7$-II]=-0.62 eV and E_{tot}^{min} [$In_2Sn_2O_7$-I]- E_{tot}^{min} [$In_2Sn_2O_7$-II]=-1.1 eV. Consequently, $In_2Ge_2O_7$-I and $In_2Sn_2O_7$-I are more stable than their counterparts $In_2Ge_2O_7$-II and $In_2Sn_2O_7$-II. The above analysis shows that stability of $In_2X_2O_7$-I depends on atomic number of X. $In_2X_2O_7$-I is less stable than $In_2X_2O_7$-II for X=C and Si whereas it is more stable for X=Ge and Sn.

Analysis of shows that the dependencies $E_{tot}(V)$ for $In_2X_2O_7$-I (X=Si, Ge, and Sn) and -II intersect each other. This result indicates that upon compressing $In_2Si_2O_7$-II it can be transformed into $In_2Si_2O_7$-I. Upon straining $In_2Ge_2O_7$-I and $In_2Sn_2O_7$-I they can be transformed into the phase -II. The pressure-induced phase transitions between $In_2X_2O_7$-I and -II is demonstrated in Fig. 3. Analysis shows that the phase transition from $In_2X_2O_7$-II

to -I occurs at pressure values 8.68 GPa for $In_2Si_2O_7$, -15.64 GPa for $In_2Ge_2O_7$, and -5.30 GPa for $In_2Sn_2O_7$ with corresponding volume variations 29, -32, and -22 $Å^3$, respectively. In scientific literature there is no report regarding phase transitions in the oxides $In_2X_2O_7$.

Bulk modulus (B_0) is the parameter characterizing compressibility of a solid. Our calculated values are presented in Table I. It is seen that the bulk modulus for $In_2X_2O_7$-I and -II are very large and are close to 216 GPa of clinopyroxene $MgSiO_3$ (Ref. [24]) existing in the Earth's deep mantle. As expected B_0 for $In_2X_2O_7$-II are smaller than that of $In_2X_2O_7$-I because of their smaller equilibrium volumes. Consequently, $In_2X_2O_7$-I are more compressible than $In_2X_2O_7$-II.

3.2. Electronic structure

The calculated band structure is plotted in Fig. 4 for $In_2X_2O_7$-I and -II. One of the important points to mention is dispersion of the bottommost CB and topmost VB. It is seen in Fig. 4 that the bottommost CB is well dispersive whereas topmost VB are almost dispersionless for $In_2X_2O_7$-I and -II. On the one hand it means that if the compound can be doped with impurities providing *n*- and *p*-type conductivity, then the electrical current transported by the CB electrons will be much larger than that by the same concentration of holes. On the other hand it indicates that the electrons in the VB are tightly bound to the O anions and that predominant ionic type of chemical bonding is present in the compounds.

One of the parameters to be determined from the band structure is the fundamental band gap E_g, which is difference energy of the bottommost CB and topmost VBs. E_g has been estimated from Fig. 4 and is summarized in Table II. Analysis

of Fig. 4 and Table II shows that $In_2X_2O_7$-I and -II except $In_2C_2O_7$-II are wide band gap oxides possessing large fundamental band gap. Here it should be mentioned the systematic DFT error in calculation of the fundamental band gap. So, the real gaps E_g of $In_2X_2O_7$-I and -II are expected to be larger than the calculated ones presented in Table II. Often rigid shift of the band gap is used to correct the error in calculated band gaps. For this aim knowledge of the experimentally measured band gap is needed. Due to lack of such experimental data rigid shift technique has not been applied.

One of the parameters, characterizing transparency of *n*-type conducting material is the difference of energies (E_g^*) between the nearest two minimums in the bottommost part of CB. Our calculations show that $E_g^* \geq 2.8$ eV for $In_2Si_2O_7$-II, $In_2Ge_2O_7$-I, and $In_2Sn_2O_7$-II. It indicates that if heavy doping with shallow donors is possible, the materials forming the interface layers in optoelectronic device structures can still be transparent to the visible part of the solar spectra.

For quantitative analysis of the band dispersion CB electron effective masses have been calculated [Table III]. Analysis shows that the calculated CB electron effective masses are comparable with those of the well known TCO materials like ZnO and ITO. CB electron effective masses are found to be almost isotropic along all directions. The calculated effective mass values are of the same order as the well known TCOs like ZnO and In_2O_3. The effective masses corresponding to the topmost VB is found to be anisotropic. Topmost VB for $In_2Ge_2O_7$-I and $In_2Si_2O_7$-I is dispersive along $\Gamma \rightarrow A$.

The total density of states (DOS) is presented in Fig. 5. The fundamental band gap, effective density of states and intrinsic carrier concentration,[25] charge neutrality level[26] can be determined can be determined from the total DOS (TDOS). Here it will be

studied for analysis of the distribution of all valence electrons, chemical bonding as well as the role of different structural modifications in electronic structure of in $In_2X_2O_7$-I and -II. It is seen in Fig. 5 that the VB for $In_2C_2O_7$ and $In_2Sn_2O_7$-I and -II consists of four major regions whereas VB for the rest $In_2X_2O_7$-I and -II consists of three regions. As demonstrated below by the analysis of orbital and site projected DOS (PDOS) the lowest region in the VB (to be called hereafter as VB1) of $In_2Sn_2O_7$-I and -II come from the Sn-4*d* electrons, which is not available in the other $In_2X_2O_7$. It is located in the energy range 17.0-18.5 eV. The VB1 for $In_2C_2O_7$ -II is also split.

The energy region located at higher energies to be called as the VB2 is in the energy range from -17.0 to -13.5 eV. It is split into narrow sharp sub-bands. The other region is VB3 located at higher energies than VB2 and it covers the range from -13.0 to 11.0 eV. It is localized and narrow. The fourth region to be denoted as VB4 is in between ~-8.0-0 eV. This region is located in broad energy range.

In order to gain more insight into the origin of the VBs and CBs the orbital and site projected DOS (PDOS) were analyzed. Since PDOS for $In_2X_2O_7$-I and –II are similar to each other, we perform analysis for $In_2Sn_2O_7$-I. Figure 6 shows the PDOS for $In_2Sn_2O_7$-I. It is seen that VB2 consists of O 2*s* strongly hybridized with *s* and *p* electrons of In and group-IV atoms. Strong contribution comes from Sn-4*d* electrons. The band is split into several sharp peaks. Among the $In_2X_2O_7$-I and –II this feature is especially well defined in $In_2Sn_2O_7$-I and -II. The VB3 consists of the well-localized very sharp peaks centered ~-12.5 eV, which is basically contributed from In 4*d* electrons slightly hybridized with *s* and *p* electrons of O and group-IV atoms. The topmost part of the VB to be called as VB4 consists of two parts: the first one is located lower energies and is

strongly contributed by the In-5*s* and -5*p* as well as *s* and *p* electrons of group-IV atoms. The other one is located at higher energies and is contributed basically by the O-2*p* electrons.

The CB edge is well dispersed and consists basically of In 5*s* electrons and *s* electrons of group-IV atoms with smaller contribution from both O 2*s*. Hence, the *s* electrons of In and group-IV atoms play an important role in the electrical conductivity through the CB minimum for all these $In_2X_2O_7$ polymorphs. Since the contribution from the O-2*s* electrons to the CB edge is smaller, one can say that they play almost no role in the effective mass of the CB electrons.

3.3. Charge density, electron-localization function, Bader and Voronoi charges

For qualitative characterization of chemical bonding between In and O as well as between O and group-IV atoms in $In_2X_2O_7$-I and -II charge-density and electron localization function (ELF) have been analysed.[27-29] Figure 7 (a) presents the charge density distribution for In-O and Ge-O bonds of $In_2Ge_2O_7$-II. The other $In_2X_2O_4$-I and -II exhibit similar features to that of $In_2Ge_2O_7$-II. It is found that the highest charge density is residing at O atoms. A large amount of localized electrons around In come because of the semicore In 4*d* electrons, which in the computations have been considered as valence electrons. The charge around group-IV atoms is smaller than that around In. The reason is that, as demonstrated by analysis of the Bader charge in the following section, the group-IV atoms donate to O more charge than In.

Bader and Voronoi charge analysis[24-26] have been performed. Although the Voronoi charge analysis commonly is used just for a sanity check we have included it into the paper because some of the group-IV atoms such as C and Si do not contain the

core charge in the pseudopoentials, i.e. the Bader maximum. As a result, in computations the Bader charge around Si atom is smaller than in the pseudopotential and that around O atoms is larger. Consequently, according to Voronoi charge, chemical bonding of zinc silicates is not as much ionic as in the case of Bader charge analysis.[30] As expected, In and group-IV atoms *X*(*X*=C, Si, Ge, and Sn) donate electrons, while O atoms accept them. Based on the amount of the transferred charges one can conclude that chemical bonding is more ionic.

Charge density analysis shows that chemical bonding is between the O atoms with nearest neighbor In and group-IV atoms. ELF analysis shows that the charge is concentrated basically around O atoms along O-*X*(*X*=C, Si, Ge, and Sn) bonds. These pictures confirm once again dominant ionic nature of the chemical bonding. This result is consistent with analysis of PDOS [Fig. 4], which shows that charge population of the site of group-IV atoms by electrons is smaller than that of the In. This result is reasonable also, because the spectroscopic electronegativity of In and Si are 1.78 and 1.90,[31] respectively. Since electronegativity of O is 3.44, ionic interaction between In and O as well as between Si and O is more enhanced than covalent bonding.

PDOS can also be useful also for qualitative analysis of the chemical bonding in $In_2X_2O_7$ polymorphs. Such analysis has been performed, which shows that the bonding mechanism in $In_2X_2O_7$ is the hybridization between In 3*p*, O 2*p* as well as *p* states of group-IV atoms in large energy range in close vicinity of the CB and VB edges. Furthermore, the non-spherical charges around the Zn, Si, and O atoms are the indications of the covalent character of the chemical bonding. The ionicity is because the

main peaks of O 2*p*, In 4*s*, and *p* states of Ge and Sn atoms are located in different energy range, because the main peaks of O and C/Si are located in different energy range.

3.4. Optical spectra

In order to describe the optical anisotropy, six diagonal components of the dielectric response function are calculated for $In_2X_2O_7$-I and one component for $In_2X_2O_7$-II. Among the six components for $In_2X_2O_7$-I, the off-diagonal components are found to be negligible and hence the analysis is made for just the three diagonal components corresponding to the electric field **E** parallel to the crystallographic **a**, **b** and **c** axes. The one component for $In_2X_2O_7$-II is because optical properties of this modification are isotropic.

It should be noted that because of the well-known deficiency of DFT to underestimate the band gaps the calculated optical spectra are shifted toward lower energies relative to the experimental spectra. Due to lack of experimentally determined band gaps and optical spectra for $In_2X_2O_7$-I and -II correction schemes have not been applied such as, e.g., rigid shift of the optical spectra toward larger energies up to the experimentally determined location.

Figure 8 displays the imaginary part of the dielectric response function for $In_2X_2O_7$-I along **E**||**a**, **E**||**b**, and **E**||**c** and $In_2X_2O_7$-II as a function of the photon energy. Analysis shows that in the photon energies >4.1 eV $\varepsilon_2(\omega)$ for $In_2C_2O_7$-II is anisotropic and it depends on crystal structure. Compared to $In_2C_2O_7$-II, $\varepsilon_2(\omega)$ for $In_2C_2O_7$-I is shifted toward lower energies because of its smaller band gap. The $\varepsilon_2(\omega)$ spectra for $In_2Si_2O_7$-II is isotropic in the energy range 0.0-4.5 eV and anisotropic at larger photon energies. Furthermore, the $\varepsilon_2(\omega)$ spectra for $In_2Si_2O_7$-I is different than that of $In_2Si_2O_7$-

II, so it depends on lattice type. In the energy range 0.0-4.2 eV optical properties of $In_2Si_2O_7$ is isotropic and is almost the same for both $In_2Si_2O_7$-I and -II. The dependency on the crystallographic directions and lattice type becomes evident at larger energies of photons. Optical spectra for $In_2Sn_2O_7$-I and -II is anisotropic and differ each from other.

Below further analysis of the optical spectra of for $In_2X_2O_7$-I other than $\varepsilon_2(\omega)$ will be performed only for one direction **E**||**a**. The absorption coefficient $\alpha(\omega)$, reflectivity $R(\omega)$, refractive index $n(\omega)$, and extinction coefficient $k(\omega)$ are presented in Fig. 9 for $In_2C_2O_7$-I, -II, $In_2Si_2O_7$-I, -II and in Fig. 10 for $In_2Ge_2O_7$-I, -II, and $In_2Sn_2O_7$-I, -II. The optical spectra can be useful in the discussions of the possibility of application of $In_2X_2O_7$-I and -II in devices, e.g., in solar cells. One of the examples is $In_2Si_2O_7$ polymorphs, which might be formed according the solid state reaction

$$In_2Si_2O_7 \Leftrightarrow In_2O_3 + 2SiO_2 \qquad (3)$$

To answer the question as to whether the intermediate layer can be used as antireflection coating or not knowledge of optical reflectivity and refractive index can be important. Analysis of Figs. 9 and 10 shows that in the energy range 0 to 4 eV, $n(\omega)$ and $R(\omega)$ of $In_2X_2O_7$-I and -II are close to those of SiN_x (Ref.[32]). Consequently, if the $In_2Si_2O_7$ is formed at the interface between Si and In_2O_3:Sn, then it can be an antireflection coating layer. Studies of defects, electrical current transport properties of $In_2X_2O_7$-I and -II and their band alignment with other semiconductors will be subject of future studies. We hope that our theoretical results will motivate experimental studies on these materials.

Conclusion

Ground state properties, electronic structure, and optical properties of $In_2X_2O_7$ (X=C, Se, Ge, and Sn) in monoclinic (-I) and cubic (-II) phases have been studied by DFT. $In_2C_2O_7$-II and $In_2Si_2O_7$-II as well as $In_2Ge_2O_7$-I and $In_2Sn_2O_7$-I are found to be most stable polymorphs. Possibility of phase transition between phases -I and -II of $In_2X_2O_7$ is shown and bulk modulus, transition pressure, and volume shrinkages have been estimated. From the band structure calculations the difference of the energy of the lowest conduction band from that of the topmost valence band has been found. Bottommost conduction band is found to be strongly dispersive whereas the topmost valence band is slightly dispersive. Effective masses of the conduction band electrons are found to be much smaller than those of the holes in the valence band. The $In_2X_2O_7$ compounds are found to be transparent in the visible part of the solar spectra. Based on magnitude of the refractive index and reflectivity $In_2X_2O_7$-I and -II are suggested to be used as antireflection coating layer in solar cells.

Acknowledgments

This work has received financial and supercomputing support from the Research Council of Norway within FUNMAT and NANOMAT projects.

References

1. Y. Messous, B. Chambon, M. De Jésus, D. Drain, C. Pastor, A. Garcia, J. P. Chaminade, T. Gaewdang, C. Fouassier, B. Jacquier and B. Varrel, Nuclear Instruments and Methods in Physics Research Section A: Accelerators, Spectrometers, Detectors and Associated Equipment **354** (2-3), 527 (1995).
2. T. J. Bukowski and J. H. Simmons, Critical Reviews in Solid State and Materials Sciences **27** (3-4), 119 (2002).
3. J. H. Simmons and T. J. Bukowski, *Final report*, Other Information: PBD: 7 Aug 2002, Report No. DOE ER45808; TRN: US200302%%654 United States10.2172/798490TRN: US200302%%654Tue Feb 05 04:43:52 EST 2008OSTI as DE00798490OAK; RN03006611English, 2002.
4. T. J. Bukowski, the University of Florida, 2002.
5. J. H. G. Simmons, FL), Patent 5720827, *Design for the fabrication of high efficiency solar cells*, University of Florida (Gainesville, FL), United States, 1998
6. J. S. Huber, W. S. Choong, W. W. Moses, J. Qi, J. Hu, G. C. Wang, D. Wilson, S. Oh, R. H. Huesman, S. E. Derenzo and T. F. Budinger, Ieee Transactions on Nuclear Science **53** (5), 2653 (2006).
7. T. E. Gier, X. Bu, P. Feng and G. D. Stucky, Nature **395** (6698), 154 (1998).
8. E. Celik, U. Aybarc, M. Ebeoglugil, I. Birlik and O. Culha, J. Sol-Gel Sci. Technol. **50** (3), 337 (2009).
9. W. Heward and D. Swenson, Journal of Materials Science **42** (17), 7135 (2007).

10. A. Martel, F. Caballero-Briones, A. Oliva, R. Castro-Rodríguez, A. Iribarren, P. Bartolo-Pérez and J. Peña, physica status solidi (b) **220** (1), 261 (2000).
11. J. H. Zhan, Y. Bando, J. Q. Hu, L. W. Yin, X. L. Yuan, T. Sekigitchi and D. Golberg, Angewandte Chemie-International Edition **45** (2), 228 (2006).
12. Y. Su, S. Li, L. Xu, Y. Q. Chen, Q. T. Zhou, B. Peng, S. Yin, X. Meng, X. M. Liang and Y. Feng, Nanotechnology **17** (24), 6007 (2006).
13. T. Gaewdang, J. P. Chaminade, P. Gravereau, A. Garcia, C. Fouassier, M. Pouchard, P. Hagenmuller and B. Jacquier, Zeitschrift Fur Anorganische Und Allgemeine Chemie **620** (11), 1965 (1994).
14. (Gmelin Institut, Karlsruhe, 2001).
15. V. I. Vavilin, E. A. Gladkikh, E. A. Soldatov, E. A. Kuz'min, V. V. Ilyukhin and N. V. Belov, Sov. Phys. Dokl. **18**, 761 (1974).
16. G. Kresse and J. Furthmüller, Phys. Rev. B **54** (16), 11169 (1996).
17. J. P. Perdew and A. Zunger, Phys. Rev. B **23** (10), 5048 (1981).
18. D. M. Ceperley and B. J. Alder, Phys. Rev. Lett. **45** (7), 566 (1980).
19. P. E. Blöchl, Phys. Rev. B **50**, 17953 (1994).
20. G. Kresse and D. Joubert, Phys. Rev. B **59** (3), 1758 (1999).
21. G. Kresse and J. Hafner, Phys. Rev. B **47** (1), 558 (1993).
22. P. Ravindran, A. Delin, R. Ahuja, B. Johansson, S. Auluck, J. Wills and O. Eriksson, Phys. Rev. B **56** (11), 6851 (1997).
23. S. Z. Karazhanov, P. Ravindran, A. Kjekshus, H. Fjellvag and B. G. Svensson, Phys. Rev. B **75** (15), 155104 (2007).
24. E. Ito, M. Akaogi, L. Topor and A. Navrotsky, Science **249** (4974), 1275 (1990).

25. S. Z. Karazhanov, A. G. Ulyashin, P. Ravindran and P. Vajeeston, Philos. Mag. **88** (16), 2461 (2008).

26. S. Z. Karazhanov, P. Kroll, E. S. Marstein and A. Holt, Thin Solid Films **Submitted** (2009).

27. G. Henkelman, A. Arnaldsson and H. Jonsson, Comput. Mater. Sci. **36** (3), 354 (2006).

28. C. F. Guerra, J.-W. Handgraaf, E. J. Baerends and F. M. Bickelhaupt, J. Comput. Chem. **25** (2), 189 (2003).

29. R. F. W. Bader, *Atoms in molecules: A Quantum Theory*. (Oxford University Press, New York, 1990).

30. S. Z. Karazhanov, P. Ravindran, H. Fjellvag and B. G. Svensson, J. Appl. Phys. **126**, 123701 (2009).

31. A. L. Allred, J. Inorg. Nucl. Chem. **17** (3-4), 215 (1961).

32. S. Z. Karazhanov, P. Kroll, A. Holt, A. Bentzen and A. Ulyashin, J. Appl. Phys. **106** (5), 053717 (2009).

33. A. F. Reid, C. Li and A. E. Ringwood, J. Solid State Chem. **20** (3), 219 (1977).

Table I Primitive unit-cell dimensions and volumes, structural parameters, bulk modulus (B_0), as well as the derivative of bulk modulus (B_0') for $In_2X_2O_7$-I and -II derived from the present DFT calculations by a search of the total energy minimum. Values given in parentheses refer to experimental data.

Compound SG	Unit cell (Å)	Atom	Site	x	Y	Z	B_0 (GPa)	B_0'
$In_2C_2O_7$-I $C1_2/m_1$	a=6.3806	In	*4g*	0.5000	0.8030	0.0000	202.6	3.93
	b=8.1913	C	*4i*	0.2068	0.0000	0.4189		
	c=4.1378	O1	*2c*	0.0000	0.0000	0.5000		
	V=212.23	O2	*4i*	0.3586	0.0000	0.6971		
	B=101.09	O3	*8j*	0.2286	0.1401	0.2394		
$In_2C_2O_7$-II $Fd\bar{3}m$	A=9.0581	In	*8a*	0.0000	0.0000	0.0000	245.7	4.7
	V=185.81	C	*8b*	0.5000	0.5000	0.5000		
		O1	*16c*	0.1250	0.1250	0.1250		
		O2	*96g*	0.4298	0.6250	0.6250		
$In_2Si_2O_7$-I $C1_2/m_1$	a=6.5679(6.6226)[a]	In	*4g*	0.5000(0.5000)	0.3074(0.3078)	0.0000(0.0000)	174.7	3.94
	b=8.5715(8.6008)[a]	Si	*4i*	0.2229(0.2188)	0.0000(0.0000)	0.4102(0.4106)		
	c=4.6945(4.7020)[a]	O1	*2c*	0.0000(0.0000)	0.0000(0.0000)	0.5000(0.5000)		
	V=257.98(261.04)[a]	O2	*4i*	0.3934(0.3848)	0.0000(0.0000)	0.7178(0.7093)		
	β=102.54(102.93)[a]	O3	*8j*	0.2363(0.2348)	0.1574(0.1491)	0.2187(0.2225)		
$In_2Si_2O_7$-II $Fd\bar{3}m$	a= 9.3808(9.4130)[b]	In	*8a*	0.0000(0.0000)	0.0000(0.0000)	0.0000(0.0000)	261.34	4.65
	V=206.37(208.50)[b]	Si	*8b*	0.5000(0.5000)	0.5000(0.5000)	0.5000(0.5000)		
		O1	*16c*	0.1250(0.1250)	0.1250(0.1250)	0.1250(0.1250)		
		O2	*96g*	0.4285(0.4272)	0.6250(0.6250)	0.6250(0.6250)		
$In_2Ge_2O_7$-I $C1_2/m_1$	a=6.5829(6.6470)[c]	In	*4g*	0.5000(0.5000)	0.3069(0.3071)	0.0000(0.0000)	162.4	4.62
	b=8.7955(8.7730)[c]	Ge	*4i*	0.2381(0.2325)	0.0000(0.0000)	0.4059(0.4075)		
	c=4.9203(4.9180)[c]	O1	*2c*	0.0000(0.0000)	0.0000(0.0000)	0.5000(0.5000)		
	V=278.73(279.99[c]	O2	*4i*	0.4147(0.4084)	0.0000(0.0000)	0.7268(7282)		
	β=101.93(102.50)[c]	O3	*8j*	0.2406(2391)	0.1672(1658)	0.2118(2121)		
$In_2Ge_2O_7$-II $Fd\bar{3}m$	a=9.6872	In	*8a*	0.0000	0.0000	0.0000	228.59	4.66
	V=227.26	Ge	*8b*	0.5000	0.5000	0.5000		
		O1	*16c*	0.1250	0.1250	0.1250		
		O2	*96g*	0.4203	0.6250	0.6250		
$In_2Sn_2O_7$-I $C1_2/m_1$	a=6.6333	In	*4g*	0.5000	0.8046	0.0000	92.8	2.00
	b=9.1708	Sn	*4i*	0.2600	0.0000	0.3957		
	c=5.3184	O1	*2c*	0.0000	0.0000	0.5000		
	V=319.00	O2	*4i*	0.4417	0.0000	0.7384		
	β=99.59°	O3	*8j*	0.2424	0.1848	0.2072		
$In_2Sn_2O_7$-II $Fd\bar{3}m$	a=10.1515	In	*8a*	0.0000	0.0000	0.0000	188.8	4.73
	V=261.53	Sn	*8b*	0.5000	0.5000	0.5000		
		O1	*16c*	0.1250	0.1250	0.1250		
		O1	*96g*	0.4068	0.6250	0.6250		

[a]Experiment.[13]
[b]Experiment.[33]
[c]Experiment.[14]

Table II. Fundamental band gap (E_g) and difference of the energy between the two lowest minimums of the CB (E_g^d) (in eV) for $In_2X_2O_7$-I and -II calculated by the DFT calculations.

	$In_2C_2O_7$		$In_2Si_2O_7$		$In_2Ge_2O_7$		$In_2Sn_2O_7$	
	I	II	I	II	I	II	I	II
E_g	2.91		3.02	2.10	2.16	1.55	1.27	0.54
E_g^*	1.87	2.26	2.37	2.81	2.89	2.62	2.70	2.82

Table III. Calculated effective masses of electrons and holes (in units of the free-electron mass m_0) for $In_2X_2O_7$-I and -II.

$In_2Si_2O_7$-I	$In_2Si_2O_7$-II	$In_2Ge_2O_7$-I	$In_2Ge_2O_7$-II
0.38 $m_e(\Gamma\rightarrow Z)$	0.36$m_e(\Gamma\rightarrow X)$	0.28 $m_h(\Gamma\rightarrow L)$	0.28 $m_h(\Gamma\rightarrow L)$
0.37 $m_e(\Gamma\rightarrow A)$	0.33 $m_e(\Gamma\rightarrow L)$	0.26 $m_e(\Gamma\rightarrow A)$	0.31 $m_e(\Gamma\rightarrow A)$
2.86 $m_h(\Gamma\rightarrow A)$		1.40 $m_h(\Gamma\rightarrow A)$	2.77 $m_h(\Gamma\rightarrow X)$
			1.07 $m_h(\Gamma\rightarrow L)$

Table IV. Atomic charges (in units of the electron charge e^-) around In, Si, Ge, and O atoms calculated according to Voronoi and Bader topological analysis for $In_2Ge_2O_7$-I, -II, $In_2Si_2O_7$-I, and -II.

	$In_2Ge_2O_7$-I		$In_2Ge_2O_7$-II		$In_2Si_2O_7$-I		$In_2Si_2O_7$-II	
	Bader	Voronoi	Bader	Voronoi	Bader	Voronoi	Bader	Voronoi
In	1.94	2.05	1.92	2.08	1.97	2.05	1.92	2.08
O1	-1.18	-1.20	-1.21	-1.28	-2.00	-1.12	-1.20	-1.3
O2	-1.21	-1.25	-1.23	-1.25	-1.69	-1.22	-1.75	-1.1
O3	-1.15	-1.14			-1.62	-1.11		
Si,Ge	2.17	2.08	2.3	2.12	4.00	1.96	4.00	1.92

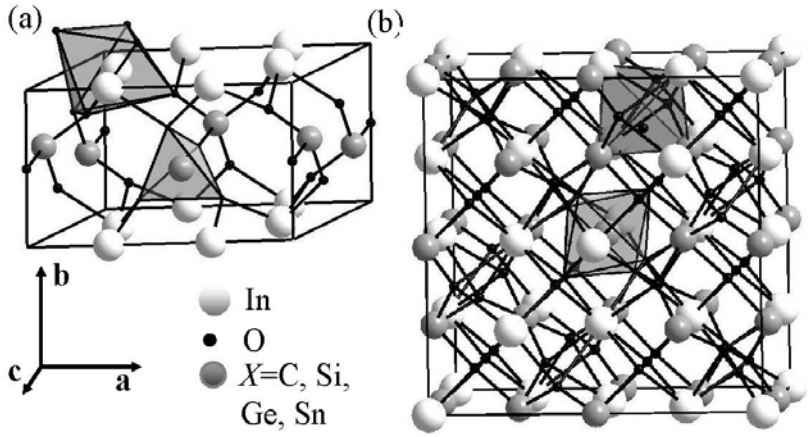

Figure 1. Crystal structure of $In_2X_2O_7$-I and –II.

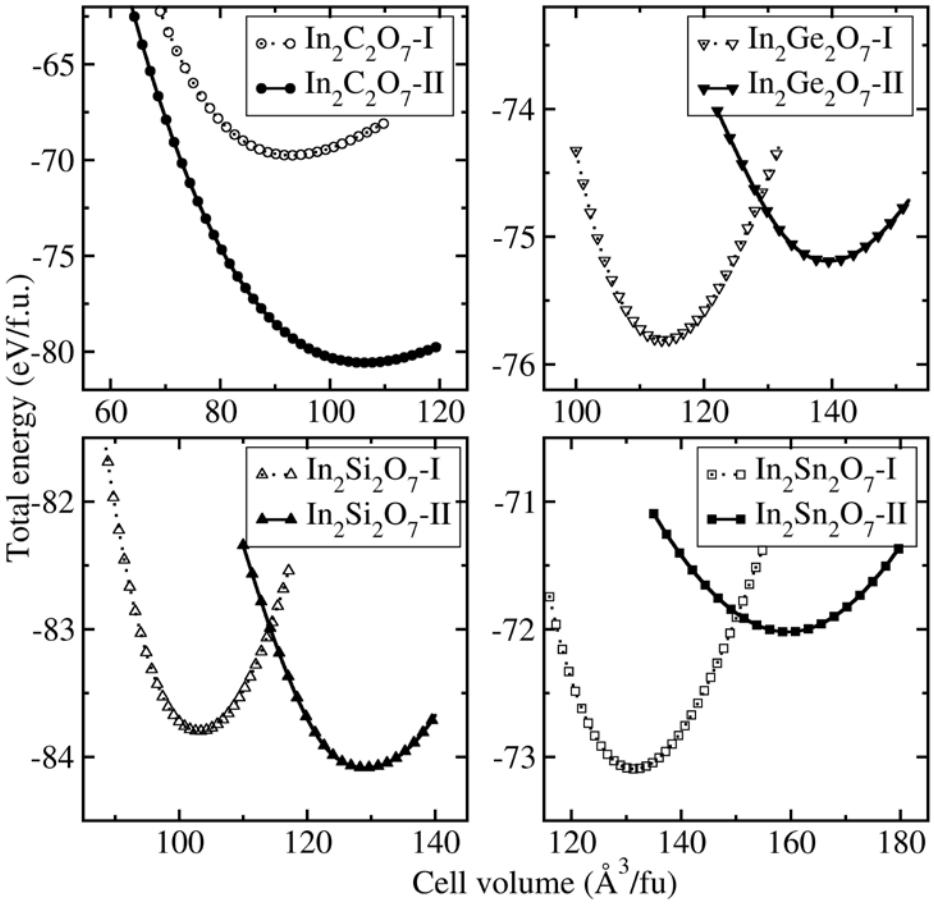

Figure 2. Dependence of total energy *Etot* on cell volume *V* per formula unit for $In_2X_2O_7$-I and II.

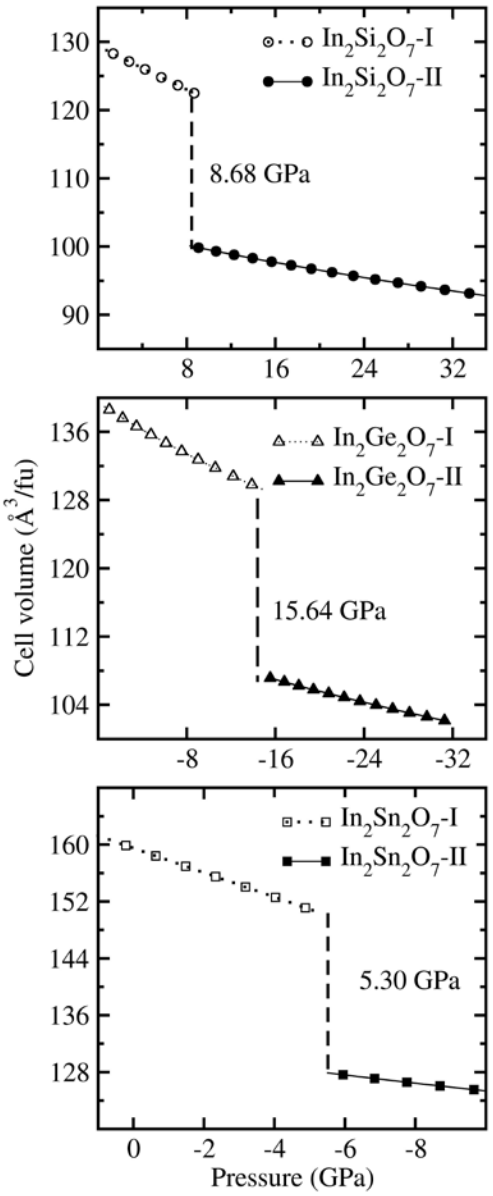

Figure 3. Calculated cell volume vs pressure for $In_2X_2O_7$-I and -II. Pressure at the transition point (in GPa) is indicated.

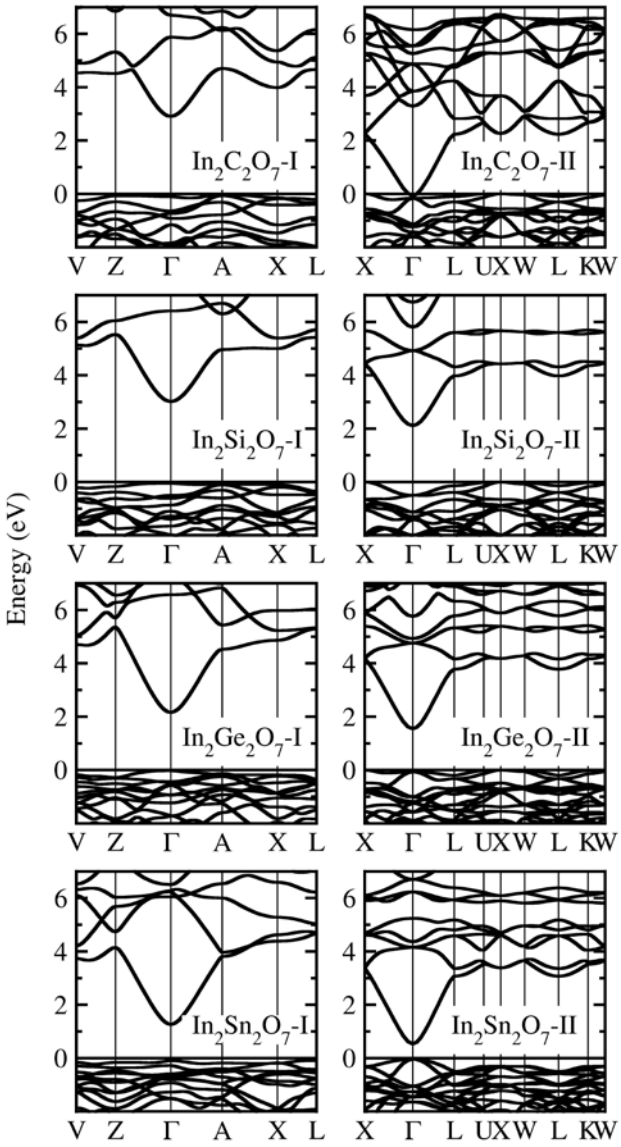

Figure 4. Band structure for $In_2X_2O_7$-I and -II polymorphs. Fermi energy is set to zero.

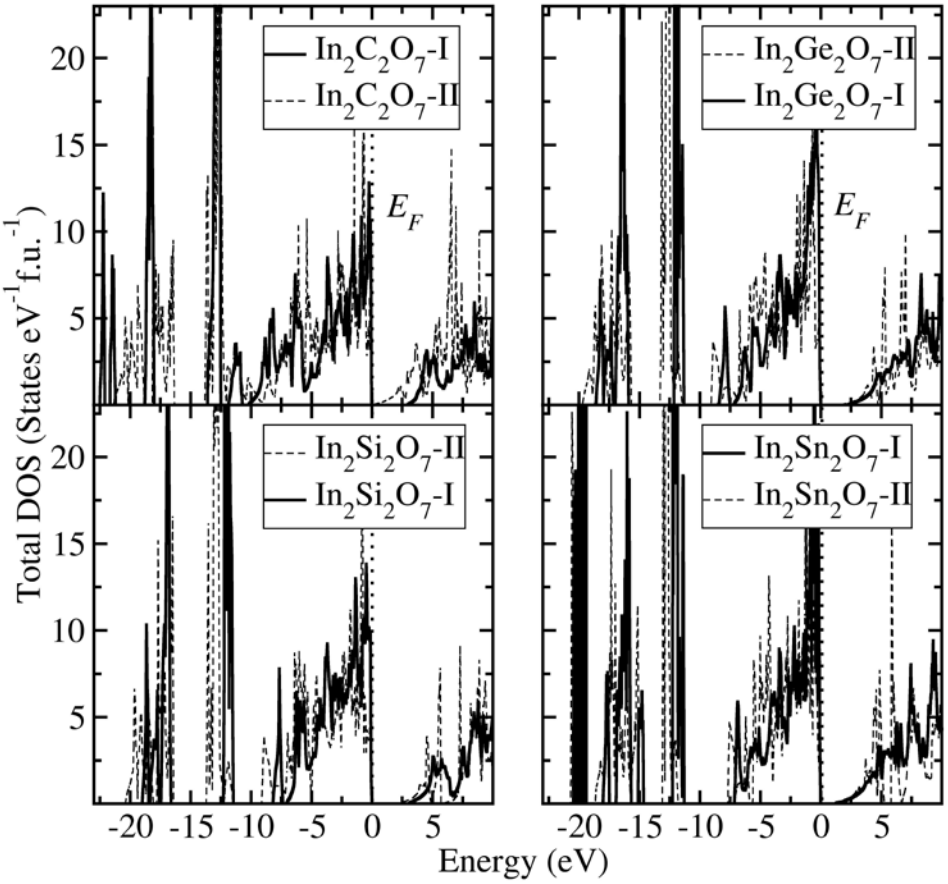

Figure 5. Total DOS for $In_2X_2O_7$-I and -II. Fermi level is set to zero.

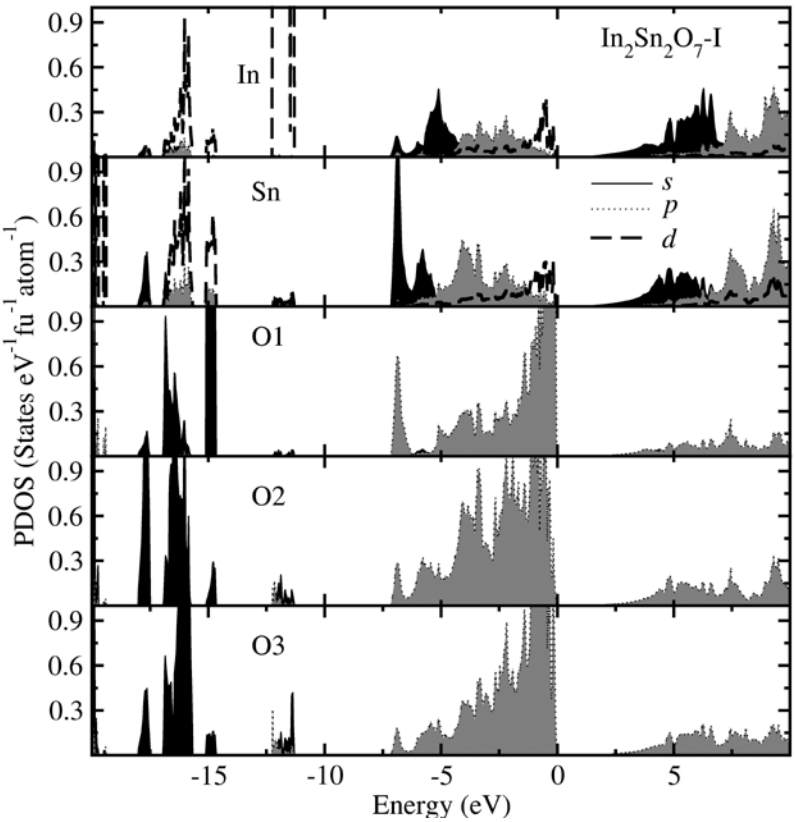

Figure 6. Orbital and site projected DOS for $In_2Sn_2O_7$-I. Fermi level is set to zero.

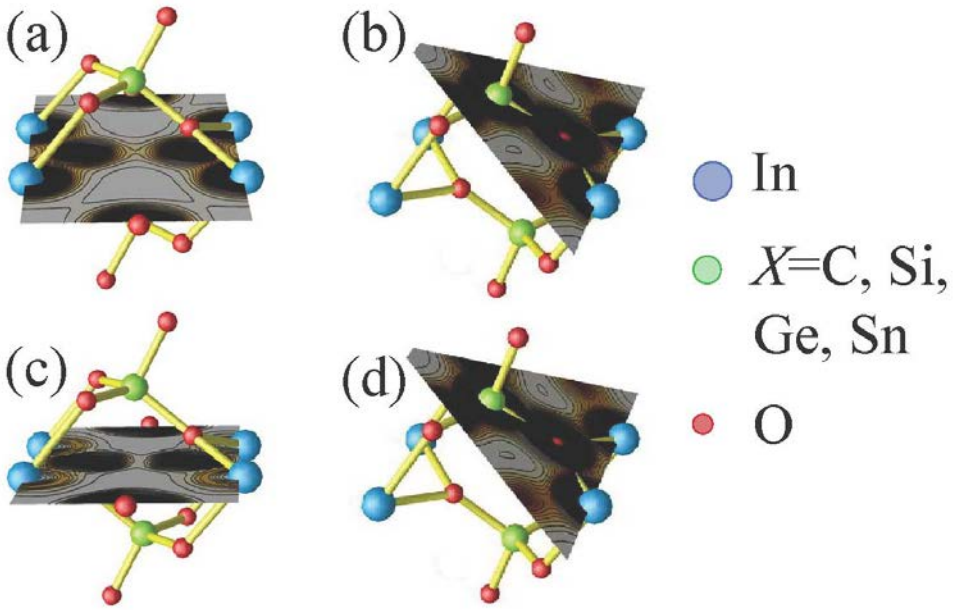

Figure 7. (a), (b) Charge density and (c), (d) ELF for $In_2Ge_2O_7$-I displaying (a), (c) In-O and (b), (d) Ge-O bonds.

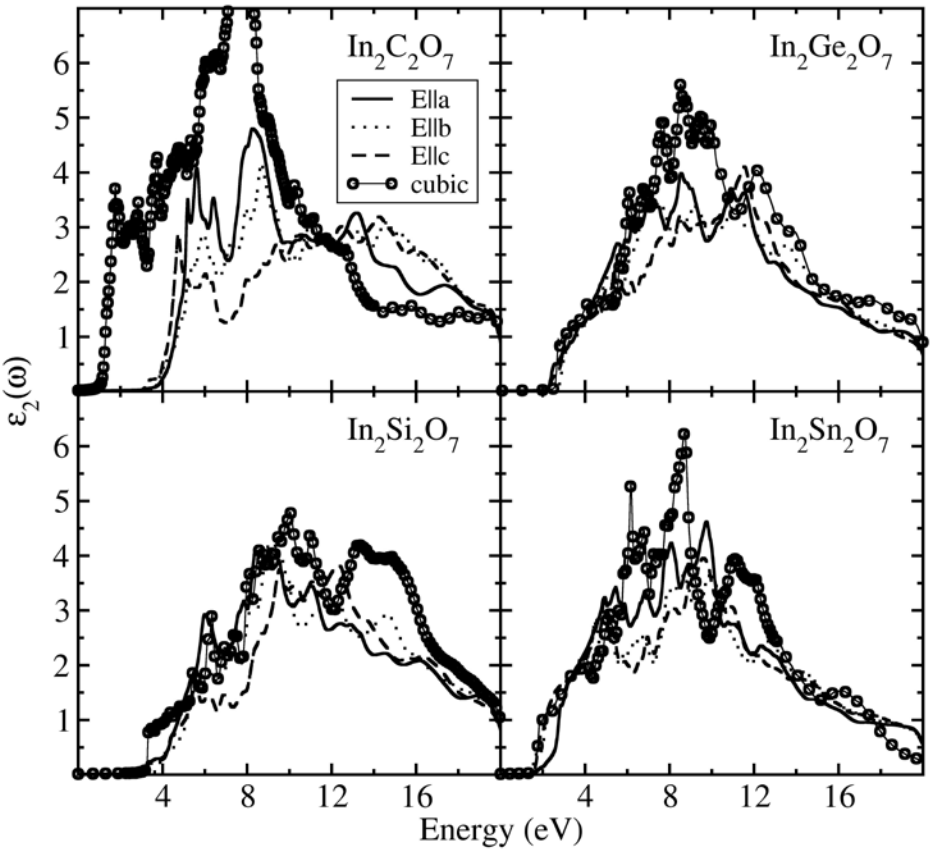

Figure 8. Imaginary part of the dielectric response functions for $In_2X_2O_7$-I (—, - - -, ·····) plotted along the **E**||**a**, **E**||**b**, and **E**||**c** directions and -II (○).

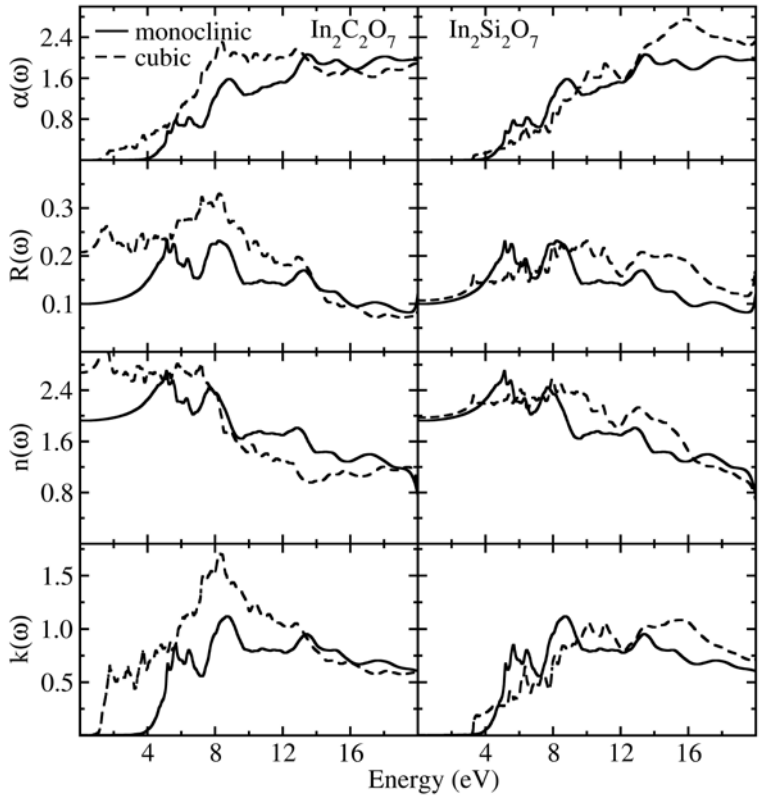

Figure 9. Calculated optical spectra of $In_2C_2O_7$ and $In_2Si_2O_7$ for the polymorphs -I (—) along the direction E||a and -II (- -). $\alpha(\omega)$ is in cm^{-1} and multiplied by 10^{-5}.

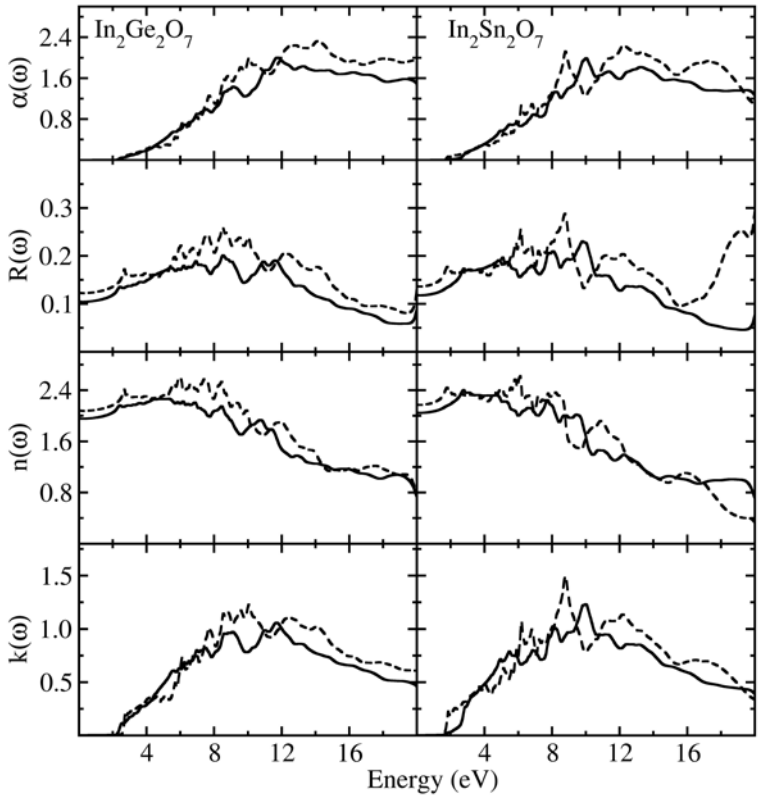

Figure 10. Optical spectra of $In_2Ge_2O_7$ and $In_2Sn_2O_7$ for the polymorphs -I (—) along the direction E||a and -II (- -). $\alpha(\omega)$ is in cm^{-1} and multiplied by 10^{-5}.